Assessing Silver Palladium Alloys for Electrochemical CO_2 Reduction in Membrane Electrode Assemblies

Chandrashekar, Sanjana; Geerlings, Hans; Smith, Wilson A.

DOI
10.1002/celc.202101258

Publication date
2021

Document Version
Final published version

Published in
ChemElectroChem

Special Collection

Assessing Silver Palladium Alloys for Electrochemical CO_2 Reduction in Membrane Electrode Assemblies

Sanjana Chandrashekar,* Hans Geerlings, and Wilson A. Smith[a]

The field of electrochemical CO_2 reduction has been transitioning to industrially relevant scales by changing the architecture of the electrochemical cells and moving away from the traditional aqueous H-cells to membrane electrode assemblies (MEA). The reaction environments in MEAs vary drastically from that of aqueous H-cells, which could result in significantly different catalytic activity. In this paper, we test AgPd alloys, one of the most promising CO producing catalysts reported, at industrially relevant scales (50 to 200 mA/cm^2) in a MEA configuration. We report that, with increasing Pd composition in the electrode, the CO selectivity reduces from 99% for pure Ag to 73% for pure Pd at 50 mA/cm^2. The MEA configuration helps attain a high CO partial current density of 123 mA/cm^2. We find that catalytic activity reported in aqueous H-Cells does not translate at higher current densities and that cell architecture must play an important role in benchmarking catalytic activity.

Introduction

Electrochemical CO_2 Reduction (ECO_2R) has gained significant interest in the past decades for its prospective role in contributing to a net-zero CO_2 society. The electrochemical conversion of CO_2 can produce valuable chemical feedstocks for the chemical industry such as CO,[1,2] formic acid[3,4] and ethylene,[5,6] By integrating this process with carbon capture technology and excess electricity generated by renewable sources, a potential net-zero carbon cycle can be established.

ECO_2R has been studied for decades in aqueous H-cell systems, and by varying parameters such as cathode composition,[7] electrolyte composition[5,8,9] and cell design,[10] it has been possible to tune the cathodic reactions to produce different products. The reaction pathways for each product vary and have different material and operational factors that affect their activity and selectivity. Of these, catalyst composition and morphology have been the most studied by the research community, as they offer diverse platforms to tune and alter reaction selectivity. Combining two metals as alloys or bimetallic catalysts with varying ratios has provided some control on the products formed showing both synergistic and deleterious effects.[11–14] In these bimetallic catalysts, Au, Ag and Cu have been primarily chosen as at least one of the metals as they have shown high selectivities for different products (Ag and Au selectively make CO, whereas Cu can produce a wide range of C_1 and C_2+ hydrocarbons).

Of particular interest in this work is the conversion of CO_2 to CO. Several combinations of metals in bimetallic and alloy catalysts have shown high selectivities for CO,[2,15,16] including AgPd alloys which have shown remarkably high selectivities for CO. Aqueous based H-Cell studies of AgPd alloys have shown its ability to outperform pure silver in their selective formation for CO.[16] Under cathodic potentials in aqueous environments, Pd has been shown to form the ß phase of its hydride which has a higher Gibbs free energy for CO adsorption as well as for the Volmer step in hydrogen evolution reaction (HER), which is proposed to be the reason for its high selectivity for ECO_2R compared to HER.[17] A similar effect has been observed with AgPd alloys where PdH forms a solid solution with Ag.[17,18] AgPd alloys have also been proposed as a candidate alloy that can approach the limit of the scaling relationship by lowering the adsorption energy for CO* more than that of COOH*.[16]

For ECO_2R to become integrated into industrial processes, a high selectivity (FE > 90%) and activity (> 200 mA/cm^2) for a single product and stability for multiple hours (> 8000 hrs),[19] at reasonable cell potentials (< 3 V) are necessary.[19] Recently, research has focused on reactor configurations that have the ability to reach > 200 mA/cm^2 using gas diffusion electrodes (GDEs) and membrane electrode assemblies (MEAs).[19,20]

Membrane electrode assemblies (Figure 1) are a zero-gap configuration where the anode, membrane and cathode are compressed together to form one reactor (Figure 1b). Gaseous CO_2 is directly fed to the electrode where it can diffuse through a porous transport layer to the catalyst surface. This zero-gap configuration allows for a very low resistance between the electrodes, while the high concentration of CO_2 helps in achieving the required high current densities. While this configuration is beneficial for scaling up this technology, it creates a reaction environment that is very different from what is found in a conventional H-cell where most catalyst screening

[a] S. Chandrashekar, Dr. H. Geerlings, Dr. W. A. Smith
Materials for Energy Conversion and Storage (MECS)
Department of Chemical Engineering
Delft University of Technology
2629 HZ, Delft, The Netherlands
E-mail: s.chandrashekar@tudelft.nl

Supporting information for this article is available on the WWW under https://doi.org/10.1002/celc.202101258

Special Collection An invited contribution to a Special Collection on Electrochemical Solar Energy Conversion and Storage.

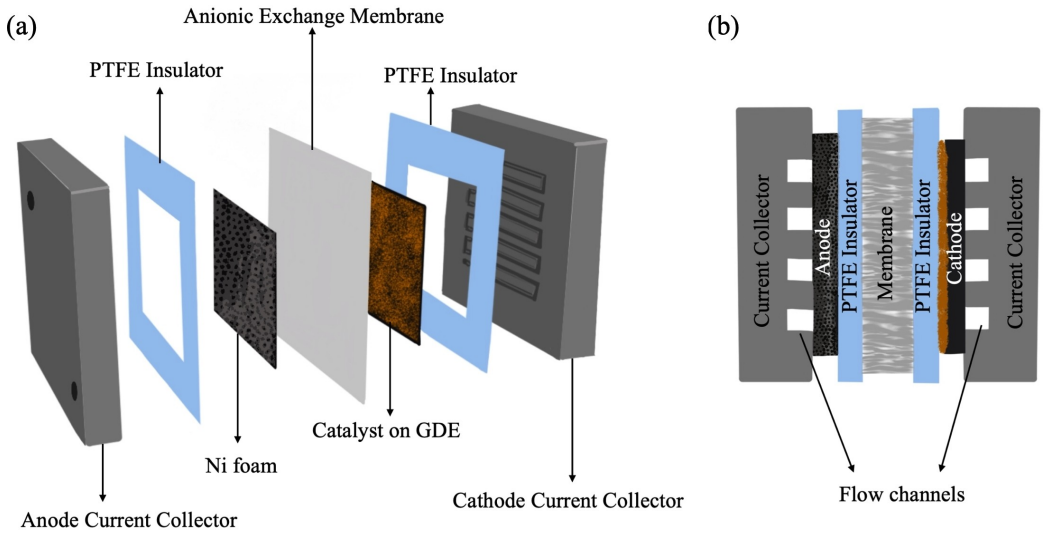

Figure 1. a) Schematic representation of a MEA. b) Cross-sectional view of an assembled MEA.

and mechanistic insights have been gained. High current densities, attainable in GDE cells and MEAs, will significantly alter the local pH, changing the catalyst activity, selectivity, and durability, while also requiring a different applied potential than for purely aqueous systems. The presence of an electrolyte membrane in direct contact with the catalyst also will affect the catalyst behaviour compared to a traditional catalyst-liquid electrolyte interface.

In this paper we use an MEA electrolyser to study one of the most promising silver alloy catalysts for CO_2 reduction, AgPd, at higher current densities than previously assessed.[16,18] Compositionally variant thin films were deposited by magnetron sputtering onto GDEs and used as catalysts and tested at current densities up to 200 mA/cm^2.The catalytic activity was found to be significantly different compared to activity reported in low current density configurations, showing the importance of screening catalysts at industrially relevant current densities and the need to bridge fundamental and applied studies of catalysts. CO selectivity is lost with increasing the Pd ratio and is suspected to be due to the architecture of the MEA cell, emphasizing the need for catalyst design and testing at high current densities with various cell architectures.

Experimental Section

Sample Preparation

RF magnetron co-sputtering was used to deposit thin films of various Ag and Pd compositions onto GDEs (Sigracet 39BC) based on the method published previously.[21] The composition of the thin films was controlled by varying the DC power supplied to the pure Ag (99.99%, MaTeck GmbH) and Pd (99.99%, MaTeck GmbH) metal targets, and the thickness was controlled by the duration of the sputtering (150 nm) and checked by a quartz crystal microbalance (QCM). Each electrode had a total geometric area of 6.25 cm^2. The different powers supplied, and the expected compositions are detailed in the Supporting Information (Table S1).

Material Characterization

X-Ray Diffraction (XRD) patterns (30°–80° 2θ) for the as-prepared samples were collected by a Bruker D8 Advance X-ray diffractometer using a cobalt source (λ = 1.7889 Å) in Bragg-Brentano configuration. After electrolysis, another diffractogram of the samples was taken to note any changes.

X-Ray Photoelectron Spectroscopy (XPS) experiments were conducted using a Thermo Scientific K-alpha apparatus equipped with an Al K-alpha X-ray Source and a flood gun to avoid charging of the sample. Parameters used for the measurements were: spot size of 400 μm, pass energy of 50 eV, energy step size of 0.1 eV, dwell time of 50 ms, 10 scans in the vicinity of Ag 3d, Pd 3d, O 1s and C 1s orbital binding energies. To obtain valence band spectra, the number of scans was increased to 100. XPS spectra were corrected using the 1 s peak from atmospheric carbon (284.8 eV).

Electrochemistry

The electrochemical conversion was conducted in a commercially available MEA setup from Dioxide Materials. Ni metal foam (Recemat BV) was used as the anode and an anion exchange membrane (AEM) (Sustainion, Dioxide Materials)[22] was placed between the anode and cathode. CO_2 was humidified upstream to the MEA and fed to the cathode at 30 ml/min. 1 M KOH was fed to the anode at 20 ml/min from a 100 ml reservoir, to maintain a constant pH of the anolyte. Such a high flowrate of anolyte was required to efficiently remove gas bubbles formed in the Ni foam. Experiments were conducted by applying a constant current density (50, 100, 150, 200 mA/cm^2) and measuring the potential over the span of 60 minutes. A new membrane electrode assembly was constructed each time with a fresh cathode and Sustainion membrane. The Ni metal foam was reused for the entire data set. The gas stream exiting the cathode was analysed every 10 min by an online Gas Chromatograph (GC) (Compact GC 4.0, GAS) with an internal N_2 reference.

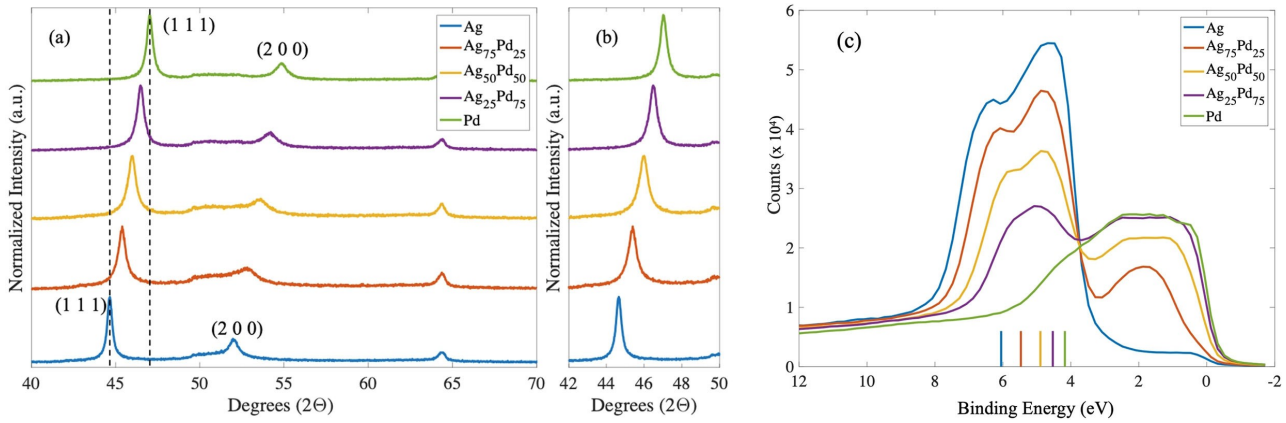

Figure 2. a, b) X-ray diffraction pattern of the different compositions synthesized. c) Valence band spectra.

Results and Discussion

To test the electrochemical performance of the AgPd alloys within a MEA architecture, it was necessary to synthesize compositionally variant catalysts on gas diffusion layers. Three compositionally variant thin film alloys of Ag and Pd along with pure Ag and Pd as control samples were fabricated on GDEs and characterized for their morphological, electronic, and compositional properties. The three intermediate compositions chosen for synthesis were $Ag_{75}Pd_{25}$, $Ag_{50}Pd_{50}$, $Ag_{25}Pd_{75}$. The following subsections discuss the material characterization of these thin films followed by their electrocatalytic performance as CO_2 reduction catalysts.

Material Characterization

Electrodes were characterized before and after electrolysis using XRD and XPS (Figure 2). XRD provides information on the bulk crystal structure of the material whereas XPS provides information over the surface composition of the catalysts along with information about metal orbital energy levels.

Figure 2 (a, b) shows the XRD patterns obtained for the as synthesized Ag, $Ag_{75}Pd_{25}$, $Ag_{50}Pd_{50}$, $Ag_{25}Pd_{75}$ and Pd. The patterns can be identified as a face centred cubic (fcc) system with (111), (200) and (220) facets being prominent for the pure Ag and Pd samples. The peaks of the intermediate compositions lie in between that of the pure metals showing the formation of alloys.[16,23] The main peak (111), shifts from 44.7° for Ag to 47.0° degrees for Pd (Figure 2b), indicating the contraction of the lattice upon introducing the smaller Pd atoms (The calculated compositions using Vegard's Law are documented in Table S2, including the change in lattice parameters).

The electrodes were also characterized after electrolysis for 60 min (Figure S1) where the ex-situ analysis depicted no splitting of the main peaks, which suggests no phase segregation occurred during ECO_2R. The appearance of additional peaks as compared to the pre-electrolysis samples can be attributed to salt formation during electrolysis in the MEA configuration (Figure S1).[24] Salts are formed at elevated current densities in such configurations due to the interaction of OH^- and CO_2, leading to the production of HCO_3^- and CO_3^- ions and eventual precipitation upon interaction with K^+ (Equations 1–3).

$$CO_2 + H_2O + 2e^- \rightarrow CO + 2OH^- \quad (1)$$

$$CO_2 + OH^- \rightleftharpoons HCO_3^- \quad (2)$$

$$HCO_3^- + OH^- \rightleftharpoons CO_3^{2-} + H_2O \quad (3)$$

Low conductivity of these ions through the anion exchange membrane (AEM) and an increased conduction of co-ions (such as K^+) from the anolyte promotes the formation of salt in and on the surface of the GDE. This can be seen with the increasing intensity of the $KHCO_3$ salt peaks with increasing current density (Figure S1). These salt formations are also visible in the SEM images taken of the catalyst surface after electrolysis (Figure S6–S10). The SEM images also show increasing salt deposits on the catalyst surface with increasing current densities. At higher current densities (200 mA/cm^2) the salt penetrated the GDE and deposited in the cathode flow channel blocking the flow of CO_2 and increasing the upstream pressure. This highlights the importance and need for better water and ion management in CO_2 electrolysis systems in general.[19,25–27]

The XPS spectra of the 3d orbitals of Ag and that of Pd are depicted in Figure S2. Figure 2c depicts the valence band structures of the alloys and pure metals, obtained from XPS. The bars at the bottom of the graph show the position of the d-band centres of the different compositions. As the concentration of Pd increased, an amalgamation of the valence band structures was observed. The d-band centre shifts closer to the fermi energy level with increasing Pd concentration, from 6 eV for Ag to 4.2 eV for Pd, a trend that has been previously observed.[16] Shifts in the peaks are attributed to the overlapping of bands in the metal atoms. Pd has shown a high affinity towards CO binding which is attributed to the position of its d-band centre in the field of heterogeneous catalysis.[28]

The process of sputtering produces GDEs that are evenly covered by the metal imitating the morphology of the micropores layer underneath (Figure S5). The SEM images (Figure S5–S10) of the catalysts, taken before and after electrolysis do not show any morphological changes occurring due to electrolysis.

Electrochemical Measurements

Chrono-potentiometric experiments were conducted on the 5 electrode compositions described, for 60 minutes, and gaseous products were analysed with an online GC every 10 min. After electrolysis at different current densities, most of the samples showed no signs of flooding except for the samples at 200 mA/cm^2 where small water droplets were seen to flow out of the cathode chamber. Product selectivity over the period of 60 minutes is

depicted in the Supporting Information (Figure S11). For the pure Ag electrode, the major product formed was CO, with the only minor product detected being H_2. The high selectivity for CO decreased from 99.5% at 50 mA/cm^2 to 62.0% at 200 mA/cm^2, while H_2 selectivity increased from 0.6% at 50 mA/cm^2 to 15.0% at 200 mA/cm^2. As the ratio of Pd increased, the selectivity for CO decreased and H_2 increased. All the alloys progressively produced less CO than Ag, contrary to what has been shown in previous literature,[18,29] while pure Pd had by far the lowest selectivity for CO (Figure 3e). For pure Pd, at 50 mA/cm^2 CO selectivity was 73.0%, which reduced to 18% at 200 mA/cm^2. Concomitantly selectivity for H_2 increased from 33% at 50 mA/cm^2 to 87.8% at 200 mA/cm^2.

For the pure Ag catalyst, other than at 50 mA/cm^2, the total faradaic efficiency (FE) for all other current densities did not add up to 100%. This may be due to the increase in selectivity for formate, as Ag has been known to produce formate at high current densities.[30,31] Direct liquid product analysis could not be conducted since there was no bulk liquid catholyte, and the suspected formate ions can easily cross over the AEM, where they can be oxidized to CO_2 at the anode.[32,33] The selectivity towards formate at the cost of CO is more likely at high cathodic potentials and high alkalinity as has been shown extensively in previous literature.[34,35] The loss in total FE was observed for other electrode compositions as well, albeit without a clear trend. It is not possible to ascertain if this is due to formate production in a MEA configuration, as a loss in total FE could also be due to H_2 absorption by the Pd.[36,37] For pure Pd, the total FE added up to almost 100% and hence it is highly likely that the Pd does not produce formate or convert to PdH at these conditions.

Figure 3e shows the cell potentials needed to obtain the applied current densities for each sample composition. These values have been averaged over 60 minutes and the chrono-potentiometric curves can be found in Figure S3. The cell potentials do not seem to have a strong dependence on the composition of the catalyst but rather on the current density applied. The cell potentials obtained here are relatively low for high current densities, as a current density of 200 mA/cm^2 was obtained at ~2.7 V, depicting the advantage of using zero gap configuration for scaling up ECO_2R.

Figure 4 depicts the partial current densities (j) of CO (Figure 4a) and H_2 (Figure 4b) at different applied current densities. All the samples have similar j at 50 mA/cm^2 and diverge at higher current densities. The partial current density for CO is highest for pure Ag, and as the concentration of Pd increases in the catalyst the j_{CO} reaches a saturation point at lower and lower current densities. However, it was observed that the j_{CO} for Pd does not increase regardless of the applied current density. This could suggest poisoning of the Pd active sites by CO, that is not related to increasing the reaction rate.[18,29]

It is likely that the CO formed by ECO_2R at the start of the flow channel, poisons the rest of the Pd catalyst under negative applied potentials, as it flows through the rest of the flow channel. The presence of CO in the gas stream reaching the catalyst as it progresses through the channel could also inhibit H_2 adsorption, limiting the formation of PdH[38] (Figure 5), the formation of which has been thought to be the reason for the high CO selectivity seen on AgPd catalysts.[16,18] The chemisorbed CO has been proposed to block H_2 dissociation sites on Pd. As more Pd gets poisoned by CO, it produces more and more H_2 propelled by the higher selectivity for HER in alkaline conditions.[39,40] Reports suggesting PdH formation aided in the increase in selectivity towards CO were conducted in cell architectures very different from that used here.

In a MEA set up, using a serpentine flow channel for the gas reactant streams will alter its composition as it moves along the channel, much like a plug flow reactor (Figure 5). It is hence essential to understand the spatial activity of the catalyst as the reactant composition changes. Furthermore, previous reports did not see such plateauing behaviour of j_{CO} on Pd, indicating that it could indeed be the MEA architecture that is responsible for the differences in activity and selectivity. More research conducted by monitoring the composition change of the gas streams at multiple

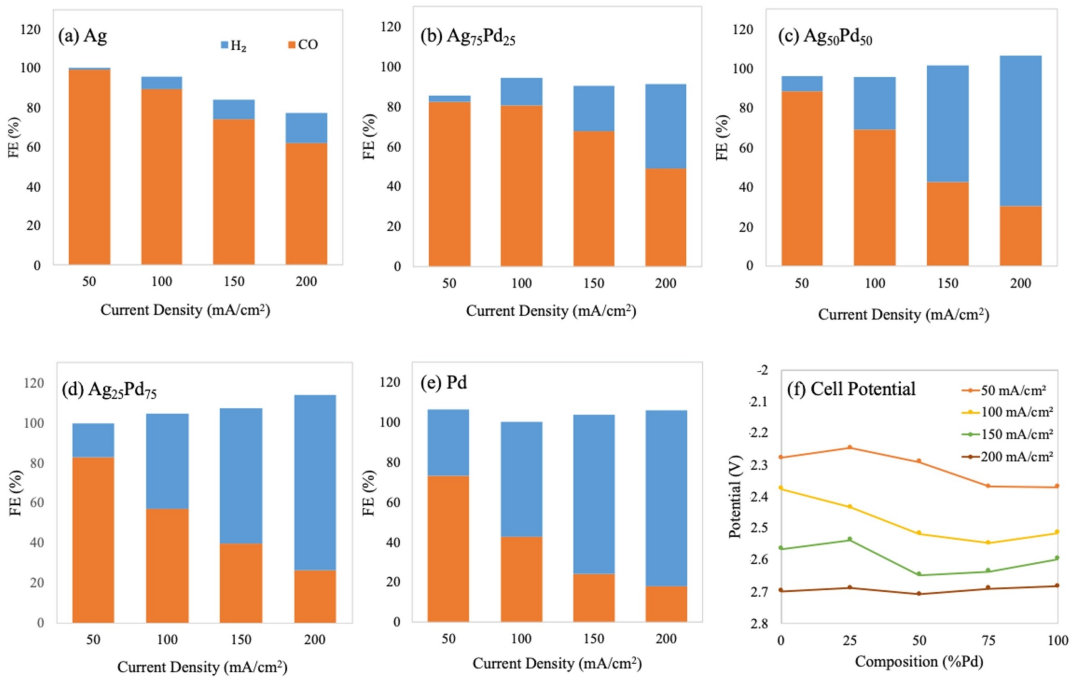

Figure 3. Average faradaic efficiency measured (over 60 minutes) at different applied current densities at constant composition a) Ag, b) Ag75Pd25, c) Ag50Pd50, d) Ag25Pd75, e) Pd. f) Cell potentials of the different compositions at constant applied current densities.

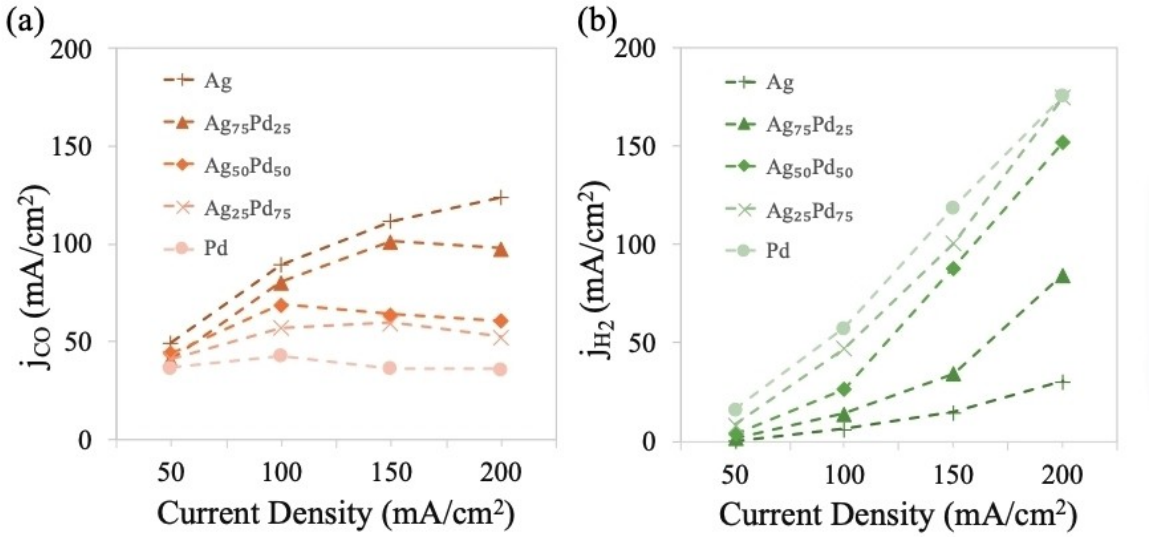

Figure 4. a) Partial current density of CO and b) H_2 as a function of applied current density.

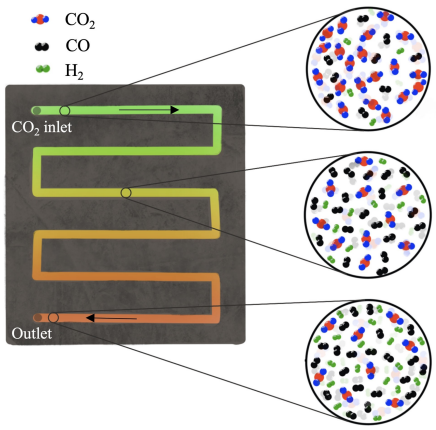

Figure 5. Schematic diagram of the cathodic current collector depicting the change in composition of the reactant stream along the serpentine flow channel.

points along the flow channel and reporting current density and FE at these points rather than an average value base only on the outlet, will aid in designing better ECO_2R electrolysers. At high current densities such as in our case, the slow kinetics for CO desorption[17] could lead to high concentrations of CO adsorbed on the surface inhibiting the formation of PdH and lowering the kinetics for CO_2 adsorption. The results presented here seem to indicate that while AgPd and PdH are suitable candidates for CO_2 reduction, this is limited to cases where the low current density and cell architecture do not allow for CO poisoning.

A carbon balance was calculated by using a N_2 internal reference to quantify the outlet products, along with the capability of the GC to quantify CO_2. This allowed for the calculation of the amount of CO_2 lost due to the cross over and the quantification of CO produced at the cathode. Figure 6a shows the outlet flowrate of CO from the cathode with a geometric surface area of 6.25 cm^2. Ag was capable of producing CO flowrates reaching up to ~5.4 ml/min at 200 mA/cm^2. Pd produces the same amount of CO at all current densities, averaging around ~1.65 ml/min.

Figure 6b shows the amount of CO_2 lost due to crossover of CO_3^-, HCO_3^-, and possibly $HCOO^-$. Which was measured by calculating the difference between the CO_2 in the inlet and the carbon products in the outlet. Under neutral and alkaline pH the protons for ECO_2R are provided by the water molecules, which leads to the conversion of CO_2 into carbonates[41] and bicarbonates which are capable of crossing the AEM to the anode (Equations 1–3).[32] It is also possible for any liquid products formed at the cathode to travel across the AEM to get oxidized at the anode to CO_2.[33] The amount of CO_2 lost due to crossover is heavily dependent on the current density applied, rather than the composition of the catalyst (Figure 6b). It is mainly the current density and CO_2 concentrations at the cathode that determine the amount of CO_2 crossing over for a particular membrane.[42] At a particular current density, the CO_2 lost to crossover is the same regardless of the composition. For Pd the loss may be slightly higher due to the higher concentrations of unreacted CO_2 at the catalyst surface. Calculating the percentage lost, about 10% of the CO_2 is lost due to crossover at 50 mA/cm^2 and as much as 35% is lost at 200 mA/cm^2. This loss of CO_2 to the anode is considerable under single pass conversions and could prove costly when scaling up as it is essentially the loss of reactants. Minimizing CO_2 crossover has to be conjugated with handling excess carbonate and bicarbonate concentrations at the cathode. For this, membrane technology, catalyst design and cell design will have to be co-designed and supplement each other's optimization pathways.[32,33,41]

Conclusions

In this paper we examine the electrochemical operation of AgPd alloys at high current densities in an MEA configuration to perform ECO_2R. Unlike what has been reported about the success of AgPd catalysts at low current densities, the same activity has not been achieved at high current densities in this configuration. This may be due to the higher production rates of CO which poison the catalyst downstream of the CO_2 inlet in the MEA. The use of a serpentine channel likely leads to CO contaminating a large part of the catalyst, inhibiting its activity. We also see that large quantities of CO_2 are lost due to

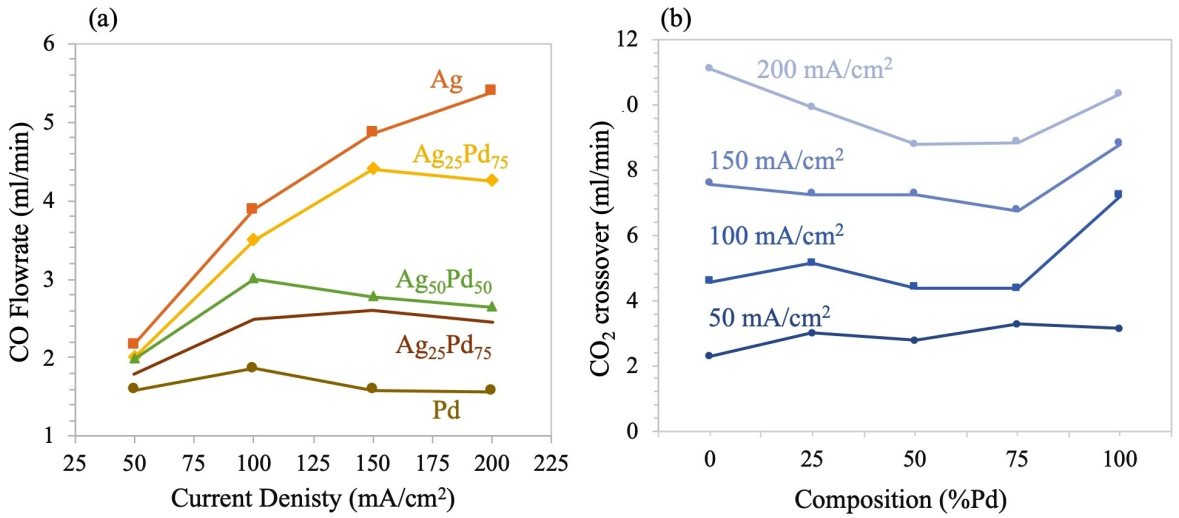

Figure 6. a) Flowrate of CO at the exit of cathode flow channel. b) Average CO_2 flowrate lost due to crossover to the anode.

membrane cross over, reducing the conversion rates of the set-up, regardless of the high current achieved. One of the reasons for the success of AgPd catalyst at low current densities was the position of the d-band centre that promoted the selectivity for CO along with the formation of PdH. If the valence band theory can be applied to high current density situations also remains in question as it could be overridden by the challenges brought on by the architecture of the MEA. It is with this knowledge that we need to encourage catalyst testing at high currents in the appropriate set ups in order to truly understand the effectiveness of the catalyst as a promising commercial catalyst.

Acknowledgements

The authors for this work would like to thank Dr. Thomas Burdyny for his support and input throughout the project. This work is part of the Advanced Research Centre for Chemical Building Blocks (ARC CBBC), which is co-founded and co-financed by the Netherlands Organisation for Scientific Research (NWO) and the Netherlands Ministry of Economic Affairs. The authors of this work are also grateful to Paul Corbett, Michiel de Heer and Maarten Schellekens for their support. The authors are also grateful to the Shell Global Solutions International B.V. for their contribution.

Conflict of Interest

The authors declare no conflict of interest.

Keywords: membrane electrode assembly · silver palladium alloys · electrocatalysis · catalytic activity · spatial activity

[1] S. Zhao, R. Jin, R. Jin, *ACS Energy Lett.* **2018**, *3*, 452–462.
[2] G. O. Larrazábal, A. J. Martín, S. Mitchell, R. Hauert, J. Pérez-Ramírez, *ACS Catal.* **2016**, *6*, 6265–6274.
[3] M. F. Baruch, J. E. Pander, J. L. White, A. B. Bocarsly, *ACS Catal.* **2015**, *5*, 3148–3156.
[4] S. Y. Choi, S. K. Jeong, H. J. Kim, I. H. Baek, K. T. Park, *ACS Sustainable Chem. Eng.* **2016**, *4*, 1311–1318.
[5] A. S. Varela, *Curr. Opin. Green Sustain. Chem.* **2020**, *26*, 100371.
[6] Y. Chen, Z. Fan, J. Wang, C. Ling, W. Niu, Z. Huang, G. Liu, B. Chen, Z. Lai, X. Liu, B. Li, Y. Zong, L. Gu, J. Wang, X. Wang, H. Zhang, J. Wang, X. Wang, H. Zhang, *J. Am. Chem. Soc.* **2020**, *142*, 12760–12766.
[7] J. He, N. J. Johnson, A. Huang, C. Berlinguette, *ChemSusChem* **2017**, *11*, 1–11.
[8] M. R. Thorson, K. I. Siil, P. J. A. Kenis, *J. Electrochem. Soc.* **2013**, *160*, DOI 10.1149/2.052301jes.
[9] X. Liu, P. Schlexer, J. Xiao, Y. Ji, L. Wang, R. B. Sandberg, M. Tang, K. S. Brown, H. Peng, S. Ringe, C. Hahn, T. F. Jaramillo, J. K. Nørskov, K. Chan, *Nat. Commun.* **2019**, *10*, 1–10.
[10] T. Burdyny, W. A. Smith, *Energy Environ. Sci.* **2019**, *12*, DOI 10.1039/c8ee03134g.
[11] S. Rasul, D. H. Anjum, A. Jedidi, Y. Minenkov, L. Cavallo, K. Takanabe, *Angew. Chem. Int. Ed.* **2015**, *54*, 2146–2150; *Angew. Chem.* **2015**, *127*, 2174–2178.
[12] D. Kim, J. Resasco, Y. Yu, A. M. Asiri, P. Yang, *Nat. Commun.* **2014**, *5*, 4948.
[13] R. Kortlever, I. Peters, S. Koper, M. T. M. Koper, *ACS Catal.* **2015**, *5*, 3916–3923.
[14] S. Chandrashekar, N. T. Nesbitt, W. A. Smith, *J. Phys. Chem. C* **2020**, *124*, 14573–14580.
[15] S. Sarfraz, A. T. Garcia-Esparza, A. Jedidi, L. Cavallo, K. Takanabe, *ACS Catal.* **2016**, *6*, 2842–2851.
[16] J. Zeng, W. Zhang, Y. Yang, D. Li, X. Yu, Q. Gao, *Appl. Mater. Interfaces* **2019**, *11*, 33074–33081.DOI 10.1021/acsami.9b11729.
[17] W. Sheng, S. Kattel, S. Yao, B. Yan, Z. Liang, C. J. Hawxhurst, Q. Wu, J. G. Chen, *Energy Environ. Sci.* **2017**, *10*, 1180–1185.
[18] J. H. Lee, S. Kattel, Z. Jiang, Z. Xie, S. Yao, B. M. Tackett, W. Xu, N. Marinkovic, J. G. Chen, *Nat. Commun.* **2019**, *10*, 1–8.
[19] D. M. Weekes, D. A. Salvatore, A. Reyes, A. Huang, C. P. Berlinguette, *Acc. Chem. Res.* **2018**, *51*, 910–918.
[20] C. T. Dinh, T. Burdyny, G. Kibria, A. Seifitokaldani, C. M. Gabardo, F. Pelayo García De Arquer, A. Kiani, J. P. Edwards, P. De Luna, O. S. Bushuyev, C. Zou, R. Quintero-Bermudez, Y. Pang, D. Sinton, E. H. Sargent, *Science* **2018**, *360*, 783–787.
[21] M. Ma, H. A. Hansen, M. Valenti, Z. Wang, A. Cao, M. Dong, W. A. Smith, *Nano Energy* **2017**, *42*, 51–57.
[22] R. B. Kutz, Q. Chen, H. Yang, S. D. Sajjad, Z. Liu, I. R. Masel, *Energy Technol.* **2017**, *5*, 929–936.
[23] T. Gunji, H. Ochiai, T. Ohira, Y. Liu, Y. Nakajima, F. Matsumoto, *Chem. Mater* **2020**, *32*, 6855–6863. DOI 10.1021/acs.chemmater.0c01137.
[24] M. Leonard, L. E. Clarke, A. Forner-Cuenca, S. M. Brown, F. Brushett, *ChemSusChem* **2019**, *13*, cssc.201902547.

[25] Y. Hori, H. Ito, K. Okano, K. Nagasu, S. Sato, *Electrochim. Acta* **2003**, *48*, 2651–2657.
[26] B. Smitha, S. Sridhar, A. A. Khan, *J. Membr. Sci.* **2005**, *259*, 10–26.
[27] J. E. Huang, F. Li, A. Ozden, A. S. Rasouli, F. Pelayo, G. De Arquer, S. Liu, S. Zhang, M. Luo, Y. Xu, K. Bertens, *Science,* **2021**, *372*, *1078*, 1074–1078.
[28] J. K. Norskov, F. Abild-Pedersen, F. Studt, T. Bligaard, *Proc. Nat. Acad. Sci.* **2011**, *108*, 937–943.
[29] T. Gunji, H. Ochiai, T. Ohira, Y. Liu, Y. Nakajima, F. Matsumoto, *Chem. Mater.* **2020**, *32*, 6855–6863.
[30] G. O. Larrazábal, A. J. Martín, S. Mitchell, R. Hauert, J. Pérez-Ramírez, *J. Catal.* **2016**, *343*, 266–277.
[31] T. Hatsukade, K. P. Kuhl, E. R. Cave, D. N. Abram, T. F. Jaramillo, *Phys. Chem. Chem. Phys.* **2014**, *16*, 13814–13819.
[32] G. O. Larrazábal, P. Strøm-Hansen, J. P. Heli, K. Zeiter, K. T. Therkildsen, I. Chorkendorff, B. Seger, *ACS Appl. Mater. Interfaces* **2019**, *11*, 41281–41288.
[33] J. Zhang, W. Luo, A. Züttel, *J. Catal.* **2020**, *385*, 140–145.
[34] E. L. Clark, S. Ringe, M. Tang, A. Walton, C. Hahn, T. F. Jaramillo, K. Chan, A. T. Bell, *ACS Catal.* **2019**, *9*, 4006–4014.
[35] C. M. Gabardo, A. Seifitokaldani, J. P. Edwards, C. T. Dinh, T. Burdyny, M. G. Kibria, C. P. O'Brien, E. H. Sargent, D. Sinton, *Energy Environ. Sci.* **2018**, *11*, 2531–2539.
[36] E. Hori, Y, Vayenas, C. G., White, R. E., Gamboa-Aldeco, M. E., *Modern Aspects of Electrochemcistry*, Springer: New York, **2008**.
[37] F. Lewis, *Platinum Met. Rev.* **1960**, *4*, 132–137.
[38] C. P. O'Brien, I. C. Lee, *J. Phys. Chem. C* **2017**, *121*, 16864–16871.
[39] W. Sheng, M. Myint, J. G. Chen, Y. Yan, *Energy Environ. Sci.* **2013**, *6*, 1509–1512.
[40] J. K. Nørskov, T. Bligaard, A. Logadottir, J. R. Kitchin, J. G. Chen, S. Pandelov, U. Stimming, *J. Electrochem. Soc.* **2005**, *152*, J23.
[41] L. C. Weng, A. T. Bell, A. Z. Weber, *Energy Environ. Sci.* **2019**, *12*, 1950–1968.
[42] N. Ziv, W. E. Mustain, D. R. Dekel, *ChemSusChem* **2018**, *11*, 1136–1150.

Manuscript received: September 15, 2021
Revised manuscript received: October 18, 2021
Accepted manuscript online: October 21, 2021